

Alma Mater Studiorum Università di Bologna
Archivio istituzionale della ricerca

The decision to go public and the IPO underpricing with locally biased investors

This is the final peer-reviewed author's accepted manuscript (postprint) of the following publication:

Published Version:

Baschieri G., Carosi A., Mengoli S. (2021). The decision to go public and the IPO underpricing with locally biased investors. EUROPEAN JOURNAL OF FINANCE, 27(15), 1489-1532 [10.1080/1351847X.2021.1890632].

Availability:

This version is available at: <https://hdl.handle.net/11585/850586> since: 2022-01-31

Published:

DOI: <http://doi.org/10.1080/1351847X.2021.1890632>

Terms of use:

Some rights reserved. The terms and conditions for the reuse of this version of the manuscript are specified in the publishing policy. For all terms of use and more information see the publisher's website.

This item was downloaded from IRIS Università di Bologna (<https://cris.unibo.it/>).
When citing, please refer to the published version.

(Article begins on next page)

This is the final peer-reviewed accepted manuscript of:

Paglianti, A.; Marotta, G.; Montante, G. Applicability of Electrical Resistance Tomography to the Analysis of Fluid Distribution in Haemodialysis Modules. The Canadian Journal of Chemical Engineering 2020, 98 (9), 1962–1972.

The final published version is available online at: <https://doi.org/10.1002/cjce.23826>.

Rights / License:

The terms and conditions for the reuse of this version of the manuscript are specified in the publishing policy. For all terms of use and more information see the publisher's website.

This item was downloaded from IRIS Università di Bologna (<https://cris.unibo.it/>)

When citing, please refer to the published version.

APPLICABILITY OF ELECTRICAL RESISTANCE TOMOGRAPHY TO THE ANALYSIS OF FLUID DISTRIBUTION IN HEMODIALYSIS MODULES

Alessandro Paglianti^{1,*}, Gaspare Marotta², Giuseppina Montante³

¹ Dipartimento di Ingegneria Civile, Chimica, Ambientale e dei Materiali, Alma Mater Studiorum – Università di Bologna, via Terracini 34, 40131 Bologna, Italy

² Medtronic, Via Camurana 1, 41037 Mirandola, Modena, Italy

³ Dipartimento di Chimica Industriale "Toso Montanari", Alma Mater Studiorum – Università di Bologna, via Terracini 34, 40131 Bologna, Italy

ABSTRACT

This work is aimed at exploring the applicability of Electrical Resistance Tomography (ERT) to the analysis of the fluid distribution in hemodialysis modules, that is not straightforward, due to the complex geometry of the hollow fiber bundles and the small size of the modules. On the other hands, ERT is potentially a suitable and convenient technique for the investigation in this field, due to its cheapness and capability to perform measurements in opaque systems. After a preliminary estimation of the fiber bundle local distribution on the measurement section, the assessment of the technique is performed by observing the time evolution of the measured conductivity maps, during the module filling and emptying operation with water and air, which are alternatively fed inside or outside the fiber bundle. Physically consistent conductivity maps are obtained placing the module vertically or horizontally. Additional experimental data collected feeding liquid mixtures of different sodium chloride concentrations show that the technique is suitable to detect concentration variations due to the mass transfer through the fibers and flow maldistribution due to the specific geometry of the module. From the preliminary results collected in this work, the technique appears to be adequate for the collection of data that can support the module geometrical optimization and computational model validation.

Keywords: Electrical Resistance Tomography, hemodialysis module, fluid dynamics, hollow fiber, dialysate.

*Corresponding Author (A. Paglianti)

1 INTRODUCTION

Dialyzers perform blood purification by hollow fiber bundles that are semi-permeable membranes for the removal of toxins, as urea and creatinine, and the excess of water. In the dialyzers, the blood flows inside the fibers while a solution called dialysate flows outside them. Nowadays hemodialysis is one of the most important treatment for blood purification during several condition of renal- or multi-organ disease. The number of the patients is continuously increasing, the social cost of the treatment is significant and the environmental impact of dialysis delivery is not negligible.^{[1],[2]} In 2010, the treatment costs accounted for 6.3% of the medical budget in USA.^[3]

Notwithstanding the increasing importance of the pathologies that require hemodialysis, the investments in research and developments have been reduced in the last few years due to the economic crisis. Catapano and Buscaroli^[4] identified three main targets for the possible improvement of the current technology: a) the physical-chemical properties of the membrane surface, b) the morphology and the chemistry of the membranes, c) the membrane module design. On this last aspect, chemical engineering investigation methods are particularly suitable, since fluid dynamics and mass transport phenomena importantly contribute to the overall dialyzer performances. The fluid dynamics of the modules has been studied by many authors in the last three decades. The experimental results obtained so far pointed out the importance of both of fluid flow characteristics within the fibers and in the dialysate compartment. The presence of non-ideal flow worsens the module performances.^{[5],[6],[7]} The flow in the two compartments presents different characteristics due to the different geometrical features of modules and membranes and to the rheology of the fluids: inside the fibers the haematocrit level has a relevant effect on the flow dynamics,^[5] while if water flows inside the fibers the velocity profile is relatively uniform.^[8] To obtain uniform flow distribution outside the fibers is more challenging, because often channeling occurs.^{[5],[6],[9],[10]} To limit the effect of flow maldistribution, the introduction of spacers or the use of crimped fibers waved to give Moiré structure are routinely used. Finally, the fibers distribution inside the module is not always homogeneous, since higher fiber density in the interior part of the bundle and lower fiber packing close to the module wall have been noticed.^[11] Obviously, if the fibers are not uniformly distributed across the section, important effects will be induced on the flow and on the driving force for the mass transfer process.

To date, the experimental data collected for the fluid dynamics analysis of the dialyzers are based on highly sophisticated techniques, which provide effective and detailed data, require specific expertise for appropriate adoption and are generally quite expensive: X rays,^{[11],[12]}

helical computed tomography,^{[5],[9]} computed tomography perfusion protocol,^{[13],[14]} magnetic resonance,^{[8],[15],[16]} MRI spin echo sequence.^[17] Also, techniques based on tracer experiments have been successful adopted providing either a visual detection of the module fluid dynamics and residence time distribution, mostly by pointwise measurements.^{[6],[18],[19]} As an alternative to experimental techniques, modelling methods might be adopted for design optimization, but the complexity of the fiber bundle geometry constitutes a serious limitation for the realistic description of the module geometry.

In this work, Electrical Resistance Tomography (ERT) is applied for the first time to a dialyzer, with the sole purpose of assessing the applicability of the technique for the fluid dynamics and mass transfer characterization of the modules. Due to the preliminary nature of the investigation, the fluids and the operating conditions do not resample those used for the patients' treatment. The module is a test unit, that was build using similar geometrical characteristics, materials and construction methods of a commercial one. The goal of the work is to test ERT as an aid for the development of new modules. The measurement method previously developed for the investigation of single-phase and gas-liquid chemical engineering equipment is adapted to the specific features of the hollow fiber module.

2 MATERIAL AND METHODS

2.1 The experimental set-up

A sketch of the investigated haemodialysis module with the main ERT instrumentation components is depicted in Figure 1.

The module, that was purposely built for the present investigation, consists of a polycarbonate cylinder of inner diameter, D , equal to 0.04 m and total length, H , of 0.264 m provided with four ports. The dialysate inlet and outlet ports are placed on the cylinder lateral wall on the same line parallel to the module axis, while the ports for the hollow fiber bundle inlet and outlet are placed on the opposite side of the two bases of conical shape. The tested bundle consists of high flux (HF) polyethersulfone hollow fibers of inner diameter equal to $200\text{ }\mu\text{m} \pm 15\text{ }\mu\text{m}$, thickness of $30\text{ }\mu\text{m} \pm 5\text{ }\mu\text{m}$ with pore sizes between 3-4 nm and sponge-like asymmetric configuration. This type of bundle is usually adopted on hemodiafiltration (HDF), adding the action of high convective flow to the diffusion used in standard hemodialysis (HD). The tested HF membrane has molecular weight retention-off (MWRO) of 8-10 kDa and molecular weight cut-off (MWCO) of 65-70 kDa. The internal surface area of the fibers is approximately equal to 1.5 m^2 . The total volume of the bundle is about 20% of the total dialyzer inner volume and the volume inside the filled fibers is the 30% of it. Therefore 50%

of the total volume of the module is available for the dialysate. The bundle was provided with spacer yarns made in Polytetrafluoroethylene homogeneously potted in groups of about 10 hollow fibers. The fiber bundle was encapsulated inside the housing using polyurethane resin to provide an inlet/outlet flow section and to avoid fluid leakage.

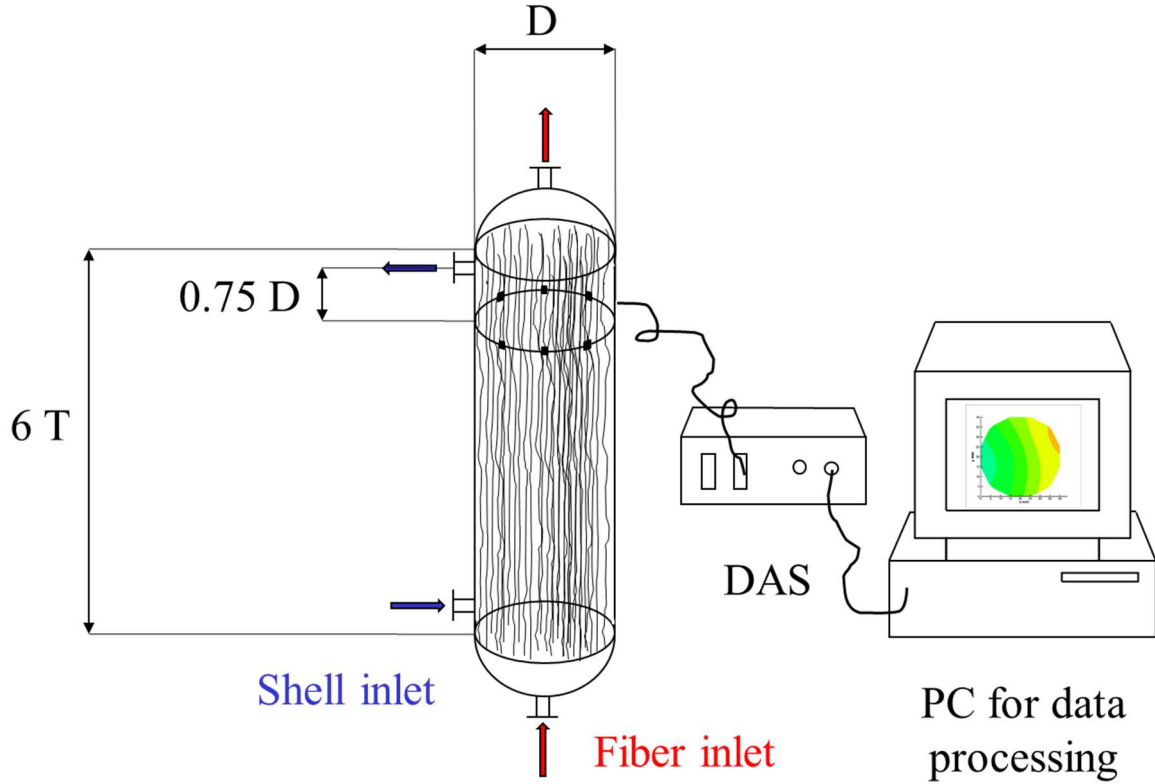


Figure 1. The hemodialyzer and the measurement system.

The ERT measurements were performed with the same ITS P2000 instrumentation (Industrial Tomography Systems Ltd) already adopted for the investigation of gas-liquid^[20] and solid-liquid stirred vessels.^[21]

By the ERT technique, the local conductivity on single or multiple cross sections of the equipment is obtained by the reconstruction of the voltage difference measurements. In this work, a single measurement plane was adopted, that was located at $0.75 D$ from the dialysate outlet port, as shown in Figure 1. For measuring the voltage difference, eight equally spaced rectangular stainless steel electrodes of size $4 \text{ mm} \times 20 \text{ mm}$ and 3 mm thickness were fixed to the module inner later wall along the circumferential plane. The electrodes were numbered as shown in Figure 2, where the vertical and the horizontal directions with the module axis placed horizontally are also indicated. Electrode 8 was located on the same tangent line as the dialysate ports.

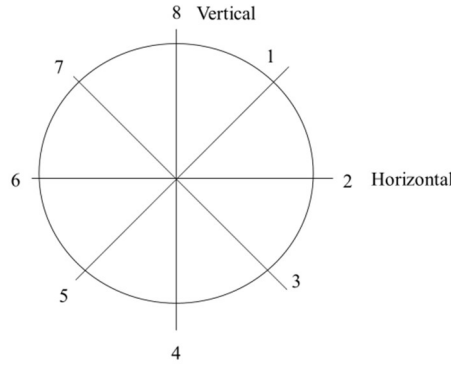


Fig. 2. The position of the electrodes.

The electrodes were connected to the Data Acquisition System (DAS) by coaxial cables, in order to reduce the signal interferences.

Different strategies can be adopted for the voltage difference measurements and for the conductivity map reconstruction. In this work, the circular adjacent strategy was employed. [22] It consists in injecting the current by an adjacent electrodes pair at a time while measuring the voltage difference from the remaining pairs of electrodes. The procedure is repeated for all pairs of electrodes. The amplitude and the frequency of the injected current were set at 15 mA and 9600 Hz respectively, after preliminary calibration tests.

As for the algorithm employed for image reconstruction, the linearized back projection algorithm was selected as implemented in the ITS System p2+ V8 software. The reconstruction of the conductivity map by means of the linearized back projection algorithm is performed in real time, thus allowing for on-line monitoring. The local conductivity (316 values per plane) was obtained on a square mesh, with cells of 2 mm x 2mm. For each set of acquisitions, up to 3000 total instantaneous measurements were collected depending on the time required to achieve the steady state condition, with an acquisition rate of 3.4 frames per second. The instrumentation allows to acquire up to 20 frames per second on multiple channels without limitations on the number of collected frames, therefore faster and longer acquisitions on multiple cross sections of the modules can be performed for a finer characterization of the modules and of the ports position both in terms of time and space resolution.

The dimensionless conductivity in the cell i at the time t , $C_i(t)$, was calculated as the conductivity measured during the experiment divided by the so-called reference conductivity. This last was measured before starting the experiments, filling both the shell and the fibers side of the module with a slightly salted liquid solution, consisting of demineralized water

with NaCl concentration equal to 0.50 g/L. The measurement reproducibility was estimated from triplicate experiments, obtaining a standard deviation of the mean dimensionless conductivity on the plane equal to 1.5%.

For the data analysis, the dimensionless conductivity is normalized as:

$$\chi_i(t) = \frac{c_i(t) - c_i(0)}{c_i(\infty) - c_i(0)} \quad (1)$$

where $\chi_i(0)=0$ and $\chi_i(\infty)=1$, with $t=0$ the starting instant of the experiment and $t=\infty$ the time corresponding to the steady state condition, irrespective of the initial and final conductivity values, therefore it is a convenient variable for comparing the fluid-dynamics behaviour in the module obtained by different measurements. Either the average value of the normalized dimensionless conductivity on the measurement plane, $\chi(t)$, or its coefficient of variation on the plane, $\text{CoV}(t)$, are observed. The coefficient of variation, CoV , of $\chi_i(t)$ is obtained as follows:

$$\text{CoV}(t) = \sqrt{\frac{\sum_{i=1}^{N_c} \left(\frac{\chi_i(t)}{\chi(t)} - 1 \right)^2}{N_c - 1}} \quad (2)$$

where N_c is the number of cells on the measurement plane.

2.2 The investigated conditions

Different experiments were performed in order to assess the applicability of the technique under various simplified conditions, by checking the consistency of the ERT data with the expected physical behaviour, namely:

- i. Spatial distribution of the fibers. In this case a solution of sodium chloride in demineralized water (salt concentration of 1.12 g/L) was continuously fed alternatively from the fiber bundle and dialysate inlet ports. The measurements were started after the achievement of the steady state conditions.
- ii. Variation of the fluid distribution inside the fibers during emptying and filling operations.
 - a. Emptying was performed feeding air from the fiber bundle inlet port. Before starting the air feed, the dialyzer was completely filled with a solution of

sodium chloride in demineralized water (salt concentration of 0.5 g/L) both outside and inside the fibers.

- b. Filling was performed starting from the steady state condition achieved at the end of the emptying operation, feeding a solution of sodium chloride in demineralized water (salt concentration of 0.5 g/L) from the fiber bundle inlet port.

The data acquisition was started simultaneously to the feeding from the inlet fiber bundle port and the conductivity maps were recorded until the steady state condition was achieved. The measurements were repeated with the horizontal and the vertical arrangements of the dialyzer.

- iii. Variation of the fluid distribution outside the fibers (namely the shell side in the following) during filling and emptying operations. The measurements were performed similarly to case (ii) feeding air (emptying) and the liquid solution (filling) from the dialysate inlet port.
- iv. Fluid distribution characteristics. In this case, the aqueous sodium chloride solution (salt concentration of 1.12 g/L) was continuously fed either from the fiber inlet or, alternatively, from the dialysate inlet in the dialyzer fully filled with a more dilute aqueous solution (salt concentration of 0.50 g/L). The data acquisition was started simultaneously to the feeding from the inlet port and the conductivity maps were recorded until the steady state condition was achieved. The measurements were repeated with the horizontal and the vertical arrangements of the dialyzer.

In all cases, the experiments were carried out at room conditions with working temperature of $25^{\circ}\text{C} \pm 2^{\circ}\text{C}$. A single pass fluid circulation was considered, to avoid any possible change of the salt concentration in the inlet solution. Air and water were fed by means of a calibrated peristaltic pump. The flow rates were approximately of the same order of magnitude of those adopted in the blood and dialysate compartments in clinical hemodialysis. Due to the preliminary purpose of this investigation, the fluids and the operations, including the filling and the emptying of the module, do not resemble those adopted in the patient's treatments.

3 ANALYSIS OF THE EXPERIMENTAL DATA

3.1 Analysis of fibers distribution

Hollows fibers distribution inside the module is one of the geometrical aspects affecting the dialyzer fluid dynamics, for this reason, ERT was firstly adopted to detect the fiber location on the measurement section. The conductivity distribution was measured after about 30 minutes of feeding 500 mL/min of an aqueous salt solution (NaCl concentration of 1.12 g/L) in the shell side or in the fibers side, for ensuring that the local conductivity values achieved steady state. In this way, the module is occupied by the same liquid in the shell side and in the fibers. The local conductivity gives information on the distribution of the fibers, that are not conductive, on the cross section of the module: zones with lower conductivity values will be characterized by higher fibers packing density with respect to zone with higher local conductivity. The measured conductivity maps shown in Figure 3 are obtained at the steady state, pumping the concentrated salt solution alternatively in the fibers side and in the shell side. As can be observed, in both cases the conductivity is not homogeneous on the section, revealing that the fibers are more closely packed close to electrodes 1 and 5, where the conductivity is lower, and they are fewer close to the electrodes 3 and 7, where the conductivity is higher.

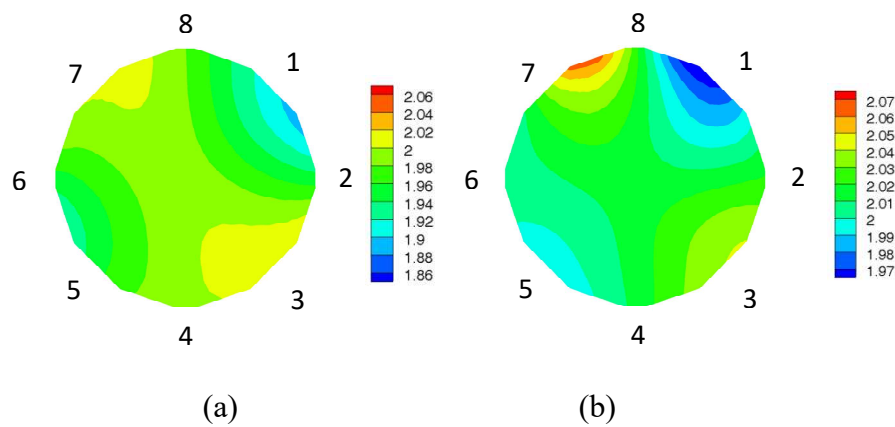


Figure 3. Dimensionless conductivity maps, measured as described in item (i) of section 2.1. a) feed from the fibers side b) feed from the shell side.

For a quantitative estimation of the fiber packing density, the conductivity maps are analysed using the following procedure.

Generally, in a system containing one conductive continuous phase and one non-conductive dispersed phase, the local volume fraction of the non-conductive material is estimated from the conductivity of the mixture compared with the conductivity of the reference obtained with

the pure continuous phase, as in the case of solid particles suspended in a stirred liquid.^[23] The conversion is often based on the simplified Maxwell equation:

$$\alpha = \frac{2(C_L - C_{mc})}{2C_L + C_{mc}} \quad (3)$$

where C_L is the dimensionless conductivity of continuous phases, that is equal to one, and C_{mc} is the dimensionless conductivity of the mixture. In the case of the dialyzer, the conversion cannot be applied directly, since the dimensionless conductivity of the continuous phase, that is usually measured when the reference condition is recorded, cannot be measured without the fibers bundle in the liquid. To overcome this limitation, the fibers packing density is estimated as the difference between the local and the mean value of the volume fraction obtained from the Maxwell equation, that reads as:

$$\alpha_i - \alpha_{mean} = \frac{2(C_L - C_i)}{2C_L + C_i} - \frac{2(C_L - C_{mean})}{2C_L + C_{mean}} \quad (4)$$

where C_i is the local measured conductivity and C_{mean} is the mean conductivity on the measured plane.

Considering that just the 20% of measurement section is occupied by the fibers, as a first approximation the mean conductivity, C_{mean} , and the pure liquid conductivity, C_L , are assumed equal. Under this assumption, Equation 4 can be rewritten as:

$$\alpha_i - \alpha_{mean} = \frac{2\left(1 - \frac{C_i}{C_{mean}}\right)}{\left(2 + \frac{C_i}{C_{mean}}\right)} \quad (5)$$

By applying Equation (5) to the cases reported in Figure 3, the deviations from the average value are equal to 0.03 and -0.014 respectively for the case reported in Figure 3a and 0.019 and -0.016 for the case reported in Figure 3b.

3.2 Analysis of the emptying and filling operations

The analysis of the conductivity maps collected during the emptying and filling operations is carried out with the purpose to evaluate first the physical consistency of the results provided by the ERT technique with the expected qualitative variations of the fluid distribution in the module. Afterwards, the specific features of the fluid distribution during both the operations

are discussed. In the following, the results are analysed considering the fiber side and the shell side, as described in items (ii) and (iii) of Section 2.1, respectively.

3.2.1 Analysis of the fibers side

The variation of the plane averaged normalized dimensionless conductivity, $\chi(t)$, measured during the emptying of the fibers with air and the filling with the aqueous salt solution when the module axis was in the horizontal position are shown in Figure 4 (a) and (b), respectively.

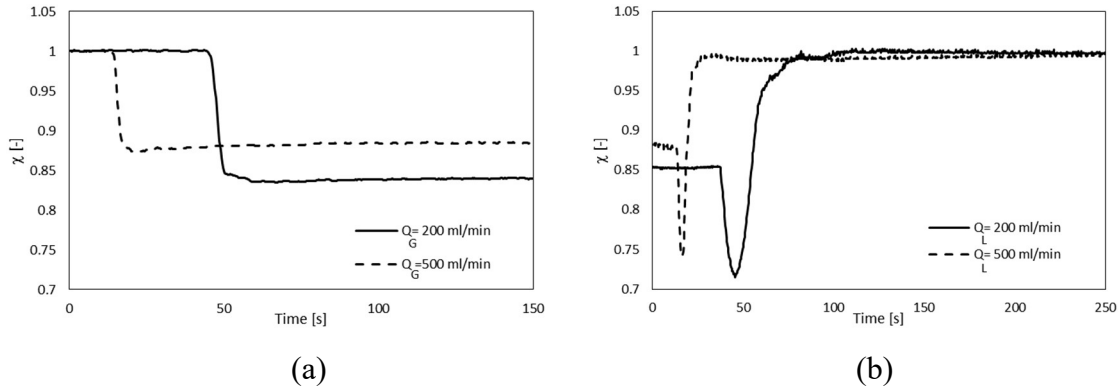


Figure 4. Time series of χ during (a) the fiber side emptying with air and (b) the fiber side filling with the aqueous salt solution. Horizontal set-up.

As can be observed in Figure 4(a), a sudden drop of conductivity is measured as soon as the air flow reaches the measurement section during the fibers emptying, that happens at different times depending on the air flow rate. The transient condition lasts a few seconds and at the steady state the two curves sit on a similar constant value. During the filling operation, the averaged dimensionless conductivity shown in Figure 4(b) exhibits a sudden drop, due to air passage in the inlet module head, and afterwards steeply increases up to the value of one when the module is completely filled with the liquid phase.

The instantaneous conductivity maps on the section, of which selected snapshots are shown in Figure 5, lead to a quantitative interpretation of the averaged curves shown in Figure 4. If the fibers would have been completely emptied, the air volume fraction inside the fibers would have been 0.3, because of the geometrical characteristics of the fibres bundle. The steady state mean dimensionless conductivities measured by ERT in the two analysed cases are equal to 0.85 and 0.88. These dimensionless conductivities are the ratio between the conductivity measured when air flows in the module and the conductivity of the module filled with the liquid phase, therefore Equation 3 can be used for the evaluation of the air volume fraction, α . In the two cases the computed values of α are 8.3% and 10.4%, that are about one third of the inner volume of the fibers. As can be observed in Figure 5, the local conductivity is not

homogeneous on the cross section. A lower value of the conductivity is achieved at steady state in the upper part of the module with respect to the bottom part, giving evidence of partial emptying of the section, as expected due to the horizontal arrangement. Indeed, the fibers side outlet port is centrally set, therefore with the horizontal set-up, the fibers located in the upper part of the module can be emptied, while below the central line the fibers remain filled with the liquid. The data recorded at the end of the emptying operation show that in the upper part of the module the local conductivity is about equal to 0.7, that using the Maxwell equation gives a volume fraction of 0.22. This value is close to the theoretical value of 0.3, suggesting that in the upper part of the module the fibers are almost filled with air. This is not a trivial result because of the geometrical characteristics of the hemodialysis module in which 20% of the volume is occupied by hollow polymeric membranes, that are characterized by low electrical conductivity, and 30% of the volume is inside the membranes, that could be shielded by the membranes. The results in Figure 5 clearly show that ERT is able to catch the changes in the electrical properties of the fluid inside the membranes.

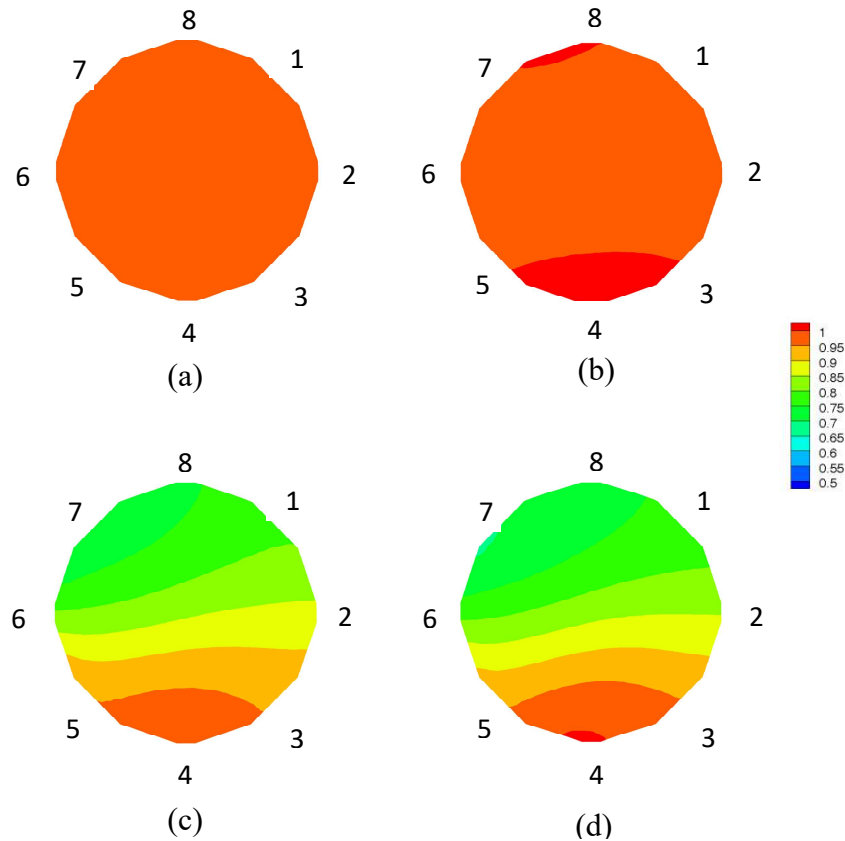


Figure 5. Snapshots of dimensionless conductivity maps during the fibers emptying operation, horizontal set-up. $Q_G = 200$ ml/min. $t = 40$ s (a) , $t = 45$ s (b) , $t = 50$ s (c) , $t = 70$ s (d).

Similarly, the conductivity map snapshots relevant to the fibers filling shown in Figure 6 provide evidence of the air passage at $t=50s$, already observed in Figure 4(b).

The expected differences obtained with the vertical set-up can be appreciated in Figure 7.

The curve recorded during the emptying operation shown in Figure 7(a) sits on a steady state value that is higher than that measured with the horizontal set-up, revealing a bigger quantity of liquid in the section with respect to the horizontal set-up. In the former case, the low shear force exerted by the gas flow on the liquid cannot overcome the gravity force acting on the liquid phase, while in the latter case the top half of the module is emptied by the gravity action. In addition, the time required for the achievement of the steady state is significantly longer with the vertical set-up, as can be observed comparing the time traces shown in Figures 4(a) and 7(a). Instead, the characteristic time of the filling operation is not affected by the module position, the main observable difference between the two arrangement that can be observed comparing the curves shown in Figure 4(b) and 7(b) is due to the passage of a big air bubble in the case of the horizontal arrangement that is absent in the vertical case giving a more regular filling in the latter configuration.

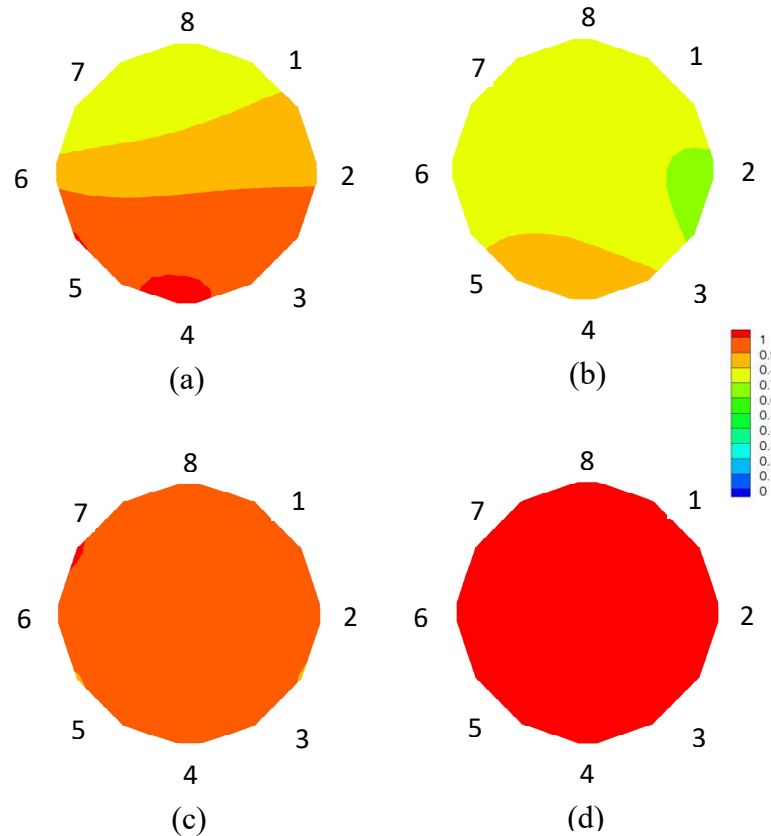


Figure 6. Snapshots of dimensionless conductivity maps during the fibers filling operation, horizontal set-up. $Q_L = 200$ ml/min. $t=35s$ (a) , $t=50s$ (b) , $t=60s$ (c) , $t=110s$ (d).

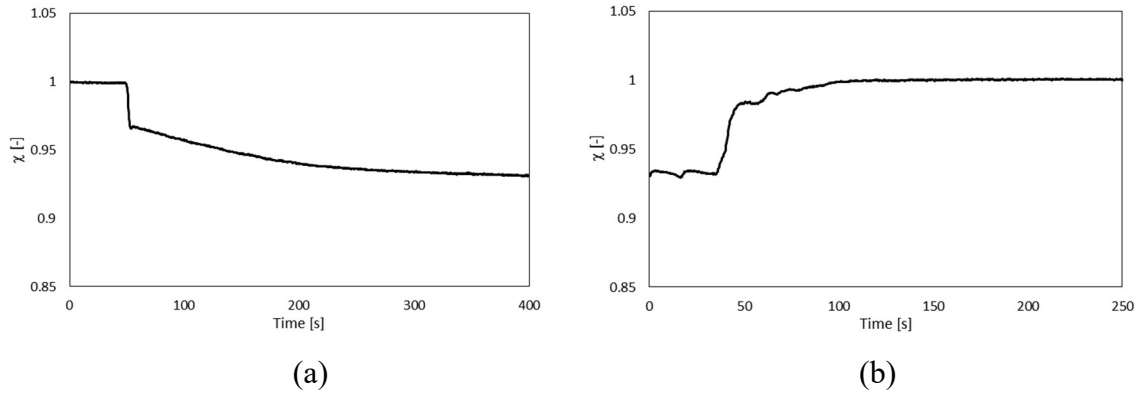


Figure 7. Time series of χ during (a) the fiber side emptying with air and (b) the fiber side filling with water. Vertical set-up, $Q_G=Q_L=200$ ml/min.

3.2.2 Analysis of the shell side

The ERT measurements during the shell side emptying and filling are more challenging than that during the same operations in the fibers, since the air passage in the shell side could electrically insulate the electrodes. The effect of air on the $\chi(t)$ curves measured during the shell emptying with air and the shell filling with the liquid is apparent in Figure 8 (a) and (b), respectively, relevant to the horizontal position of the module.

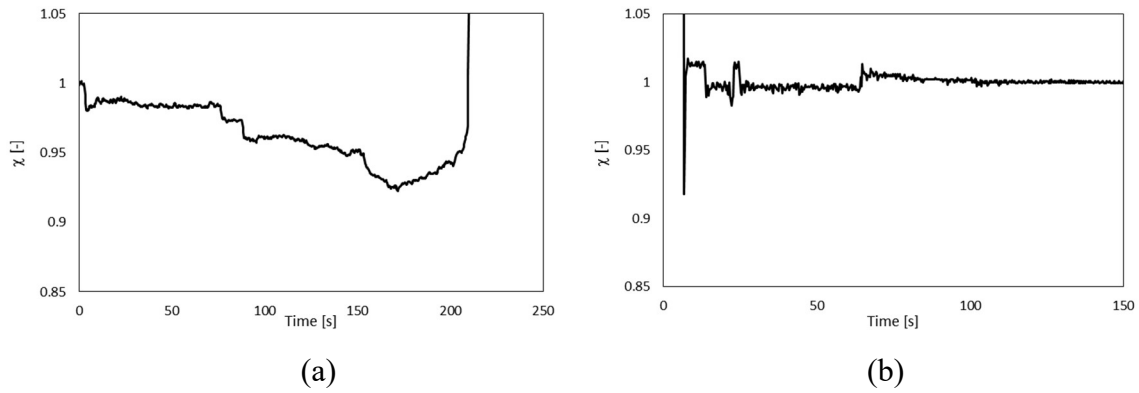


Figure 8. Time series of χ during (a) the shell side emptying with air and (b) the shell side filling with the aqueous salt solution. Horizontal set-up. $Q_G=Q_L=500$ ml/min.

As can be observed, χ exhibits a sharp increase at the end of the emptying with air and at the beginning of the filling with the liquid, when the value of the mean conductivity is largely greater than one. It is worthwhile noticing that the value of normalized conductivity equal to one means that the module is completely filled with the liquid phase, values greater than one should be due to a phase characterized by a conductivity larger than that of the salt solution used as reference, this is obviously wrong. Selected snapshots of the conductivity maps obtained during the emptying operation are shown in Figure 9.

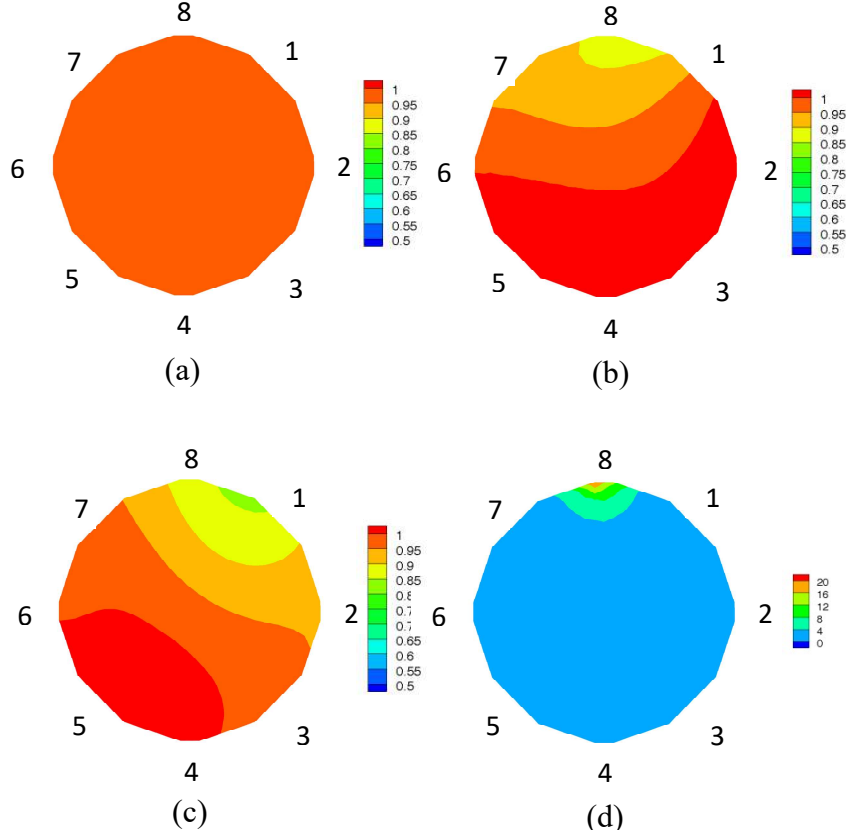


Figure 9. Snapshots of dimensionless conductivity maps during the shell emptying operation, horizontal set-up. $Q_G = 500$ ml/min. $t=50$ s (a), $t=100$ s (b) , $t=200$ s (c), $t=250$ s (d).

The maps allow the identification of the origin of the unphysical results evidenced by the time trace shown in Figure 8. Until $t=200$ s from the beginning of the experiments, the conductivity in the module is decreasing because of the presence of air that is stratified in the upper part of the module. At $t=250$ s, a gas bubble insulates the electrode 8, that is that positioned of the upper tangent line, and an unphysical solution is obtained by the algorithm that reconstructs the conductivity map from the measured voltage. Clearly, the limit of the ERT is that it can provide physical consistent results only when each electrode is in contact with a conductive phase.

The time series of χ during the shell emptying and the filling operations is shown in Figure 10 for the vertical set-up. With respect to the horizontal arrangement, during the emptying the flow pattern inside the module changes from a stratified regime to a bubbly regime. As a result, the time trace shown in Figure 10(a) fluctuates due to the bubbles transit on the measuring plane. It is interesting to notice that the maximum reached when the two phases are simultaneously present in the measuring plane is greater than one, that is clearly impossible,

because the mean conductivity of gas-liquid mixture cannot be greater than that of the liquid phase.

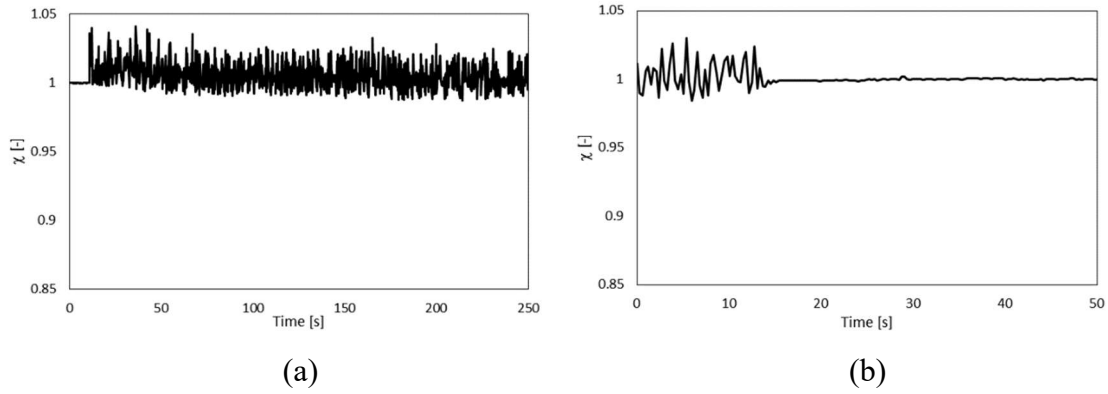


Figure 10. Time series of χ during (a) the shell side emptying with air and (b) the shell side filling with water. Vertical set-up. $Q_G=Q_L=200$ ml/min.

As shown in Figure 10(b), the filling is completed quickly, in fact the transient condition lasts about 15 seconds, afterwards, the curve becomes constant and equal to one, meaning that the measuring section is filled with the liquid phase. The snapshots shown in Figure 11 during the emptying operation provide a clearer evidence of the location of air on the section. It is possible to notice that the normalized conductivity in the opposite side of the outlet port is equal to one, that means that just the liquid phase is present. Close to the electrode 8, that is the zone where both the inlet and the outlet ports are positioned, the normalized conductivity is greater than one, meaning that air insulates the electrodes close to the outlet port.

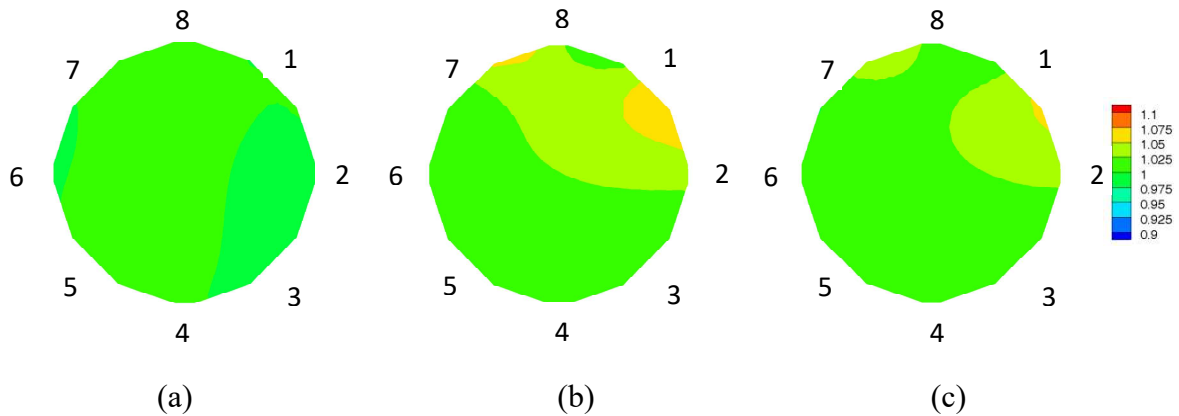


Figure 11. Snapshots of dimensionless conductivity maps during the shell emptying operation, vertical set-up. $Q_G=200$ ml/min. $t=10$ s (a), $t=20$ s (b), $t=40$ s (c).

3.3 Analysis of the module filled with liquids with different salt concentration

The fluid distribution characteristics inside the fibers and in the shell side as analysed adopting the procedure summarized in Section 2.1, item (iv) can be observed in the snapshots shown in Figure 12 and 13, respectively, both relevant to the horizontal arrangement of the module. In the experiments, the shell ports were closed when the membranes side was fed, while the lumen ports were closed in the opposite case.

The maps depicted in Figure 12 show that the dimensionless conductivity on the cross section increases with time and it does not exhibit appreciable gradients, meaning that the salt concentration changes in time, but the concentration gradients on the measuring plane are negligible.

The analysis of the snapshots shown in Figure 13 clarifies that, as a difference with the case of the flow inside the fibers, the fluid flow in the shell side experiences appreciable gradients. The local dimensionless conductivity is higher close to the electrode 8, where the inlet and outlet ports are set. Assuming a linear dependence between the local conductivity and the salt concentration it implies that, for instance at $t=200s$, the maximum value is 230% higher than the minimum one. Similar results were obtained with the vertical module position, not shown for brevity.

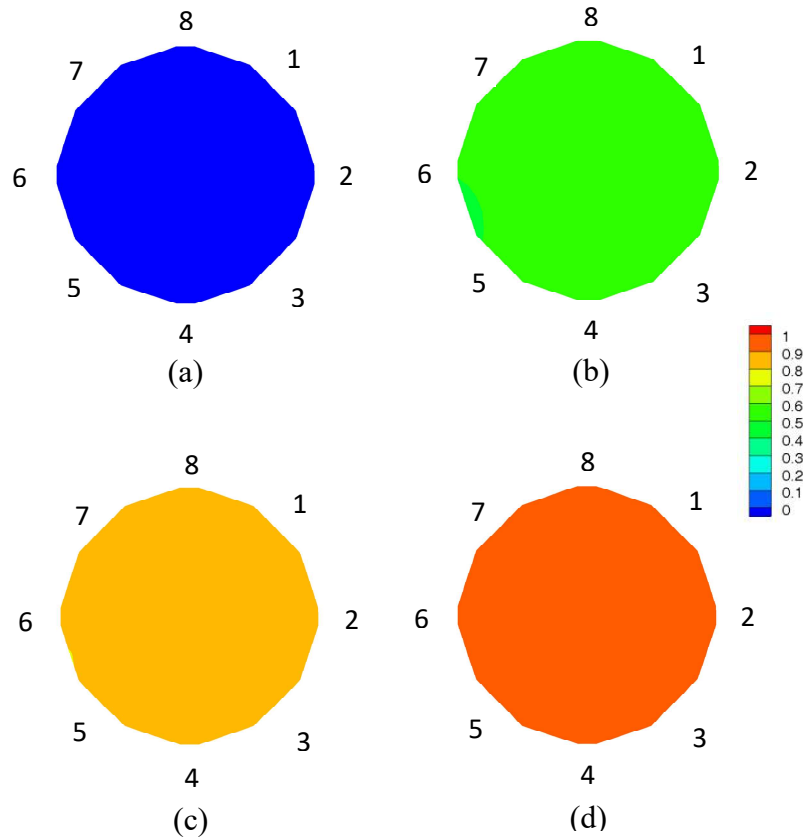


Figure 12. Snapshots of dimensionless conductivity maps during the feed of concentrated aqueous salt solution in the fibers, horizontal set-up. $Q_L = 500$ ml/min. $t=5s$ (a), $t=50s$ (b), $t=100s$ (c), $t=150s$ (d).

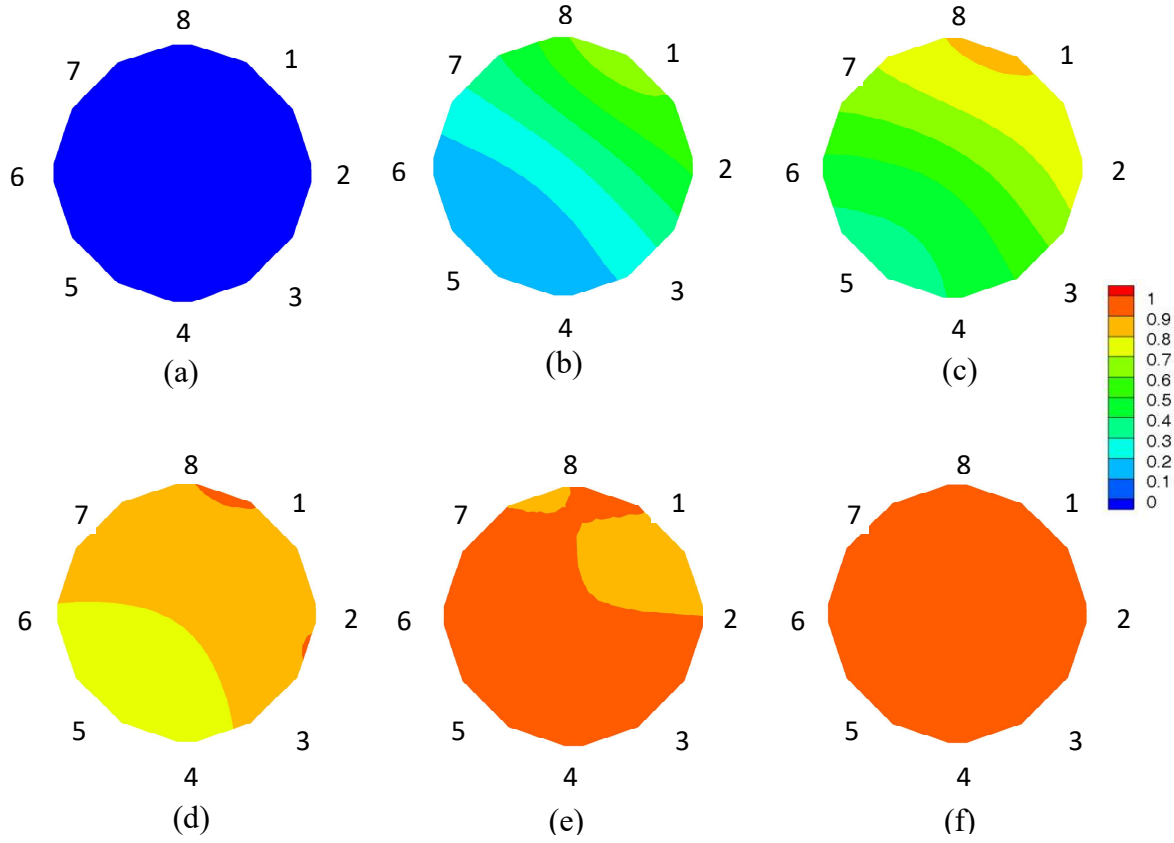


Figure 13. Snapshots of dimensionless conductivity maps during the feed of concentrated aqueous salt solution in the shell, horizontal set-up. $Q_L = 200$ ml/min. $t=20s$, $t=100s$, $t=200s$, $t=400s$, $t=700s$, $t=900s$.

The plane averaged time traces during the feeding of the concentrated aqueous salt solution in the fibers either located horizontally or vertically depicted in Figure 14 clearly show that the transient time to achieve the steady state condition is shorter the higher is liquid flowrate (Figure 14a) and the orientation does not influence the behavior of the module (Figure 14b). The experimental data obtained in the shell side are shown in Figure 15.

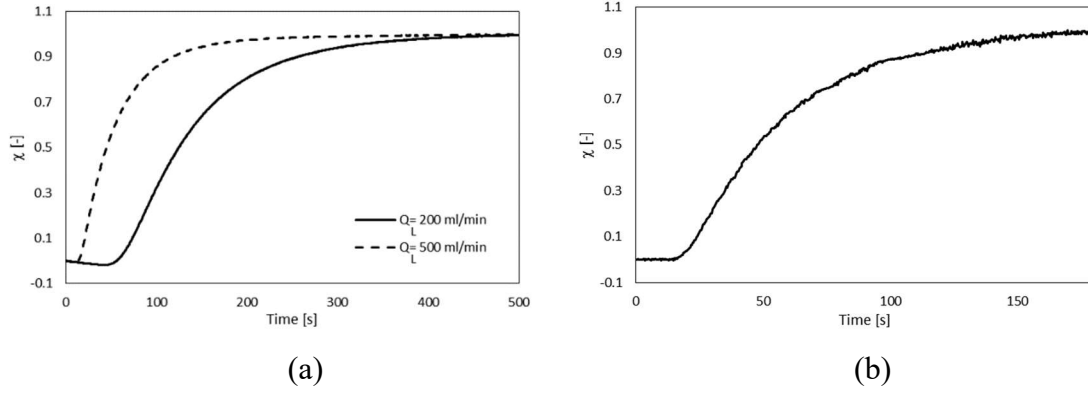


Figure 14. Time series of χ during the feeding of the concentrated aqueous salt solution in the fibers. (a) Horizontal set-up (b) Vertical set-up. $Q_L = 500$ ml/min.

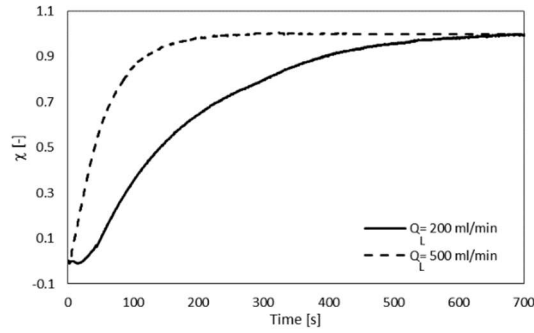


Figure 15. Time series of χ during the feeding of the concentrated aqueous salt solution in the shell side, horizontal set-up.

The experimental time series shown in the Figures 14 and 15 can be easily interpolated by using simple mass transfer equations, based on lumped parameters, or on more accurate model available in the literature.^[24]

The characteristic time required for the achievement of homogeneity on the cross section can be estimated by means of the CoV time traces calculated by Equation (2) and shown in Figure 16. The CoV peak at the beginning of the experiments detects the entrance of the concentrated solution on the measurement plane while the value of CoV equal to 0.01 has been assumed as the threshold for identifying when appreciable gradients of concentration are absent on the cross section.

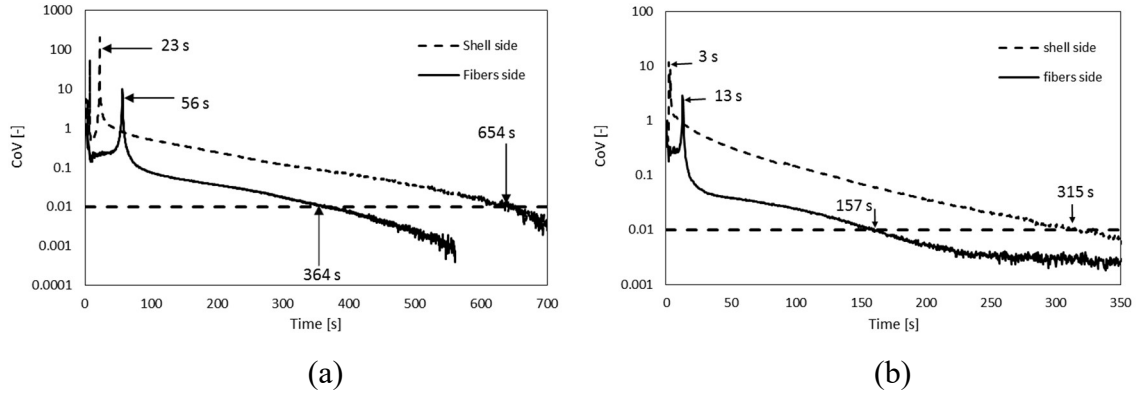


Figure 16. CoV time series during the feeding of the concentrated aqueous salt solution in the fibers and in the shell side with horizontal set-up. (a) $Q_L=200$ ml/min, (b) $Q_L=500$ ml/min.

As can be observed in Figure 16a, the CoV curve exhibits a peak at 56 s when the liquid is fed to the fibers side and at 23 s when the liquid is fed to the shell side. The difference is due to the different volume of the pipes used for connecting the fibers and the shell to the feeding tank. The homogenization times can be evaluated as $654-23=631$ s for the shell side and $364-56=308$ s for the fibers side. The analysis of the experimental data obtained increasing the liquid flow rate, shown in Figure 16b, evidences that the homogenization time, both for the fibers and the shell side, decreases to $157-13=144$ s and $315-3=312$ s, respectively, because of the increment of the mass transfer coefficient due to the increment of the liquid velocities.

It is worth observing that if the concentrated solution flows in the fibers side the time necessary for reaching the homogenization of the local conductivity, and therefore the homogenization of the salt concentration, is lower than that measured when the concentrated solution flows in the shell side. This behaviour suggests that the mass transfer from the fibers to the shell occurs differently with respect to that in the opposite direction, possibly because in the fibers the fluid moves as a plug flow, while channeling occurs in the shell side, as shown in Figure 13. The channelling in the shell side, that reduces the mean driving force for the mass transfer, gives rise to longer time for reaching homogenization of the conductivity on the measuring plane. This experimental result shows that the by-pass of the liquid phase can be caused not only from a maldistribution of the hollow fibers, but also from the inlet effects due by the port location.

Overall, the analysis of the experimental results shows that the ERT technique provides physically consistent results for the analysis of the fluid distribution and mass transfer characteristics of the dialyzers.

4 CONCLUSION

In this work, it was successfully shown that ERT can be used for evaluating the fibers distribution, for following the distribution of the fluid during transient and steady state conditions and for testing the fluid-dynamic behavior both for fibers and dialysate compartments. The analysis of the tested module has shown that the fluid flow inside the fibers can be fairly described by the plug-flow model. On the contrary, in the dialysate compartment the experimental data evidenced that channeling occurs and a significant recirculation loop of the liquid inside the shell side of the module takes place. The consistency of the collected data with those expected based on physical considerations is demonstrated. Future work will be addressed to extend the application to fluids and experimental conditions close to clinical treatments and to exploit the experimental data for computational models development and validation.

REFERENCES

- [1] J.W.M. Agar, *Hemodial. Int.* **2013**, *17*, 474.
- [2] K.A. Barraclough, A. Gleeson, S.G. Holt, J.W.M. Agar, *Nephrology* **2019**, *24*, 88.
- [3] V. Jha, G. Garcia-Garcia, K. Iseki, Z. Li, S. Naicker, B. Plattner, R. Saran, A.Y.-M. Wang, C.-W. Yang, *Lancet* **2013**, *382*, 260.
- [4] G. Catapano, A. Buscaroli, *Int. J. Artif. Organs* **2017**, *40*, 313.
- [5] C. Ronco, A. Brendolan, C. Crepaldi, M. Rodighiero, M. Scabardi, *J. Am. Soc. Nephrol.* **2002**, *13*, S53.
- [6] I. Noda, D. G. Brown-West, C. C. Gryte, *J. Membrane Sci.* **1979**, *5*, 209.
- [7] J. K. Park, H. N. Chang, *AIChE J.* **1986**, *32*, 1937.
- [8] J. Zhang, D.L. Parker, J.K. Leypoldt, *ASAIO J.* **1995**, *41*, M678.
- [9] C. Ronco, M. Scabardi, M. Goldoni, A. Brendolan, C. Crepaldi, G. La Greca, *Int. J. Artif. Organs* **1997**, *20*, 261.
- [10] C. Ronco, A. Brendolan, C. Crepaldi, M. Rodighiero, P. Everard, M. Ballestri, G. Cappelli, M. Spittle, G. La Greca, *Int. J. Artif. Organs* **2000**, *23*, 601.
- [11] A. Frank, G.G. Lipscomb, M. Dennis, *J. Membrane Sci.* **2000**, *175*, 239.
- [12] A. Frank, G.G. Lipscomb, M. Dennis, *Chem. Eng. Commun.* **2001**, *184*, 139.
- [13] J.C. Kim, J.H. Kim, H.-C. Kim, K.G. Kim, J.C. Lee, E. Kang, H.C. Kim, B.G. Min, C. Ronco, *Int. J. Artif. Organs* **2008**, *31*, 553.
- [14] J.C. Kim, J.H. Kim, H.-C. Kim, E. Kang, K.G. Kim, H.C. Kim, B.G. Min, C. Ronco, *Int. J. Artif. Organs* **2008**, *31*, 944.
- [15] S. Laukemper-Ostendorf, H.D. Lemke, P. Blümmler, B. Blümich, *J. Membrane Sci.* **1998**, *138*, 287.
- [16] C.K. Poh, P.A. Hardy, Z. Liao, Z. Huang, W.R. Clark, D. Gao, *ASAIO J.* **2003**, *49*, 440.
- [17] B.S. Weerakoon, T. Osuga, *Appl. Magn. Reson.* **2016**, *47*, 453.
- [18] I. E., De Napoli, G. Catapano, *Int. J. Artif. Organs* **2010**, *33*, 381.
- [19] G. Catapano, M. Euler, J. D. S. Gaylor, J. Gerlach, *Int. J. Artif. Organs* **2001**, *24*, 102.
- [20] G. Montante, A. Paglianti, *Chem. Eng. J.* **2015**, *279*, 648.
- [21] C. Carletti, G. Montante, C. De Blasio, A. Paglianti, *Chem. Eng. Sci.* **2016**, *152*, 478.
- [22] F. Dickin, M. Wang, *Meas. Sci. Technol.* **1996**, *7*, 247.
- [23] C. Carletti, G. Montante, T. Westerlund, A. Paglianti, *Chem. Eng. Sci.* **2014**, *119*, 53.
- [24] J. D. Brotherton, P. C. Chau, *Biotechnol. Prog.* **1996**, *12*, 575.